

## Accepted Manuscript

Title: Nitrogen-doped carbon cobalt grafted on graphitic carbon nitride catalysts with enhanced catalytic performance for ethylbenzene oxidation

Author: Xiu Lin Sufang Zhao Yuan Chen Lingling Fu  
Runliang Zhu Zhigang Liu



PII: S1381-1169(16)30126-1  
DOI: <http://dx.doi.org/doi:10.1016/j.molcata.2016.04.004>  
Reference: MOLCAA 9848

To appear in: *Journal of Molecular Catalysis A: Chemical*

Received date: 2-2-2016  
Revised date: 31-3-2016  
Accepted date: 4-4-2016

Please cite this article as: Xiu Lin, Sufang Zhao, Yuan Chen, Lingling Fu, Runliang Zhu, Zhigang Liu, Nitrogen-doped carbon cobalt grafted on graphitic carbon nitride catalysts with enhanced catalytic performance for ethylbenzene oxidation, Journal of Molecular Catalysis A: Chemical <http://dx.doi.org/10.1016/j.molcata.2016.04.004>

This is a PDF file of an unedited manuscript that has been accepted for publication. As a service to our customers we are providing this early version of the manuscript. The manuscript will undergo copyediting, typesetting, and review of the resulting proof before it is published in its final form. Please note that during the production process errors may be discovered which could affect the content, and all legal disclaimers that apply to the journal pertain.

**Nitrogen-doped carbon cobalt grafted on graphitic carbon  
nitride catalysts with enhanced catalytic performance for  
ethylbenzene oxidation**

Xiu Lin <sup>a</sup>, Sufang Zhao <sup>a</sup>, Yuan Chen <sup>a</sup>, Lingling Fu <sup>a</sup>, Runliang Zhu <sup>b</sup>, Zhigang Liu <sup>a,\*</sup>

<sup>a</sup> School of Chemistry and Chemical Engineering, Hunan University, Changsha,  
Hunan, 410082, China

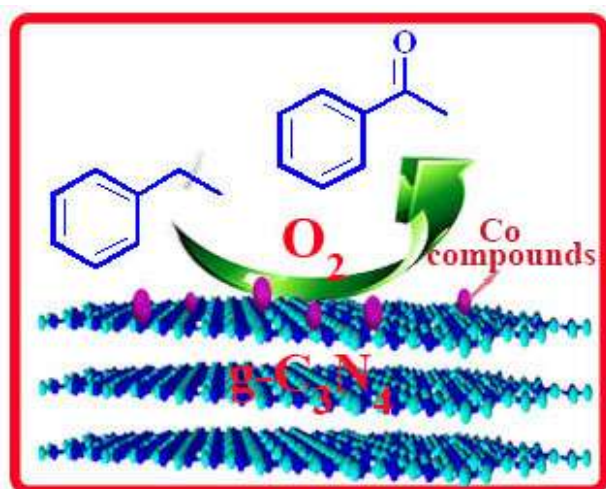
<sup>b</sup> Guangdong Provincial Key Laboratory of Mineral Physics and Material Research &  
Development, Guangzhou Institute of Geochemistry, Chinese Academy of Sciences,  
Guangzhou 510640, China

\*Corresponding author: Zhigang Liu, School of Chemistry and Chemical Engineering,

Hunan University, Changsha 410082, PR China, Tel.: +86-731-8882-3327, E-mail

address: liuzhigang@hnu.edu.cn (Z.G. Liu)

## Graphical abstract



## Highlights

- Cobalt embedded nitrogen-doped carbon grafted on graphitic carbon nitride.
- Pyrolysis of cobalt tetraphenylporphyrin (CoTPP) immobilized on graphitic carbon nitride in N<sub>2</sub> atmosphere.
- The remarkable catalytic activity and stability of Co-N-C/g-C<sub>3</sub>N<sub>4</sub> for ethylbenzene oxidation.
- Synergistic effect between Co-N-C and g-C<sub>3</sub>N<sub>4</sub>.

## Abstract

Nitrogen-doped carbon cobalt (Co-N-C) grafted on graphitic carbon nitride (g-C<sub>3</sub>N<sub>4</sub>) catalysts (Co-N-C/g-C<sub>3</sub>N<sub>4</sub>) were synthesized *via* pyrolysis of cobalt (II) 5,10,15,20-tetraphenylporphyrin (CoTPP) immobilized on graphitic carbon nitride in N<sub>2</sub> atmosphere. These catalysts were characterized by techniques such as UV-vis, FT-IR, TG-DTA, XRD, SEM, TEM, HRTEM, BET and XPS. The catalytic performance of Co-N-C/g-C<sub>3</sub>N<sub>4</sub> for selective oxidation of ethylbenzene has been investigated. As a result, when the mass ratio of CoTPP to g-C<sub>3</sub>N<sub>4</sub> is 20%, the conversion of ethylbenzene over Co-N-C/g-C<sub>3</sub>N<sub>4</sub> is 28.0%, nearly 2.3 and 1.9 times than those over pure g-C<sub>3</sub>N<sub>4</sub> and Co-N-C, respectively. Moreover, better stability is also performed after 6 runs (*i.e.*, 20.3% conversion of ethylbenzene and 71.1% of selectivity to acetophenone). The results show that the superior catalytic activity and stability maybe attributed to the Co-N<sub>x</sub> active site and the synergistic effect between Co-N-C and g-C<sub>3</sub>N<sub>4</sub>.

Keywords: Co-N-C, g-C<sub>3</sub>N<sub>4</sub>, Co-N<sub>x</sub> active site, Synergistic effect, Cobalt porphyrin, Selective oxidation of ethylbenzene

## 1. Introduction

Nitrogen-doped carbon catalysts have been drawing more and more attention from various fields of science and technology due to their chemical, electrical, functional properties and wide availability [1-3]. For the conversion of chemical raw materials and the production of fine chemicals with high value, catalytic reduction and oxidation reactions at nitrogen-doped carbon catalysts surfaces constitute one of the most significant methods [4,5]. Acetophenone, an important intermediate for the production of resins, esters, alcohol, perfumes, aldehydes and pharmaceuticals, can be synthesized in various ways [6-8]. Traditionally, acetophenone can be obtained *via* Friedel-Crafts acylation of aromatic hydrocarbons employing acid halides or acid anhydrides as reagents, with inorganic oxidants such as permanganate or dichromate and inorganic catalysts like  $\text{AlCl}_3$  [9]. However, these reactants and catalysts are not only expensive but also produce byproducts with security problems [10]. In recent decades, it is of great interest to develop a more efficient, reusable, secure and environmental friendly catalyst for the production of acetophenone.

Transition metal (Co, Fe, Mn) coordinated with nitrogen-doped carbon catalysts (M-N-C), as a type of excellent heterogeneous catalyst, are among the most promising alternative for noble-metal-based catalysts such as Pt or Pd based catalyst, owing to their abundant, low-cost, availability, durability and resistance to the methanol [11,12]. M-N-C can be obtained by the pyrolysis of mixtures containing N-rich monomers or polymers, carbon materials and metal salt [13]. In addition, porphyrin, a most widely available organic compound, can be utilized as a precursor affording C and N simultaneously. In our previous work, we have reported that an alternative method to prepare M-N-C *via* pyrolysis of composites with transition metal, nitrogen and carbon, for example, metalloporphyrin [14]. However, pure M-N-C catalysts possess poor catalytic activity for organic redox reaction [15], while M-N-C with modification of support can significantly enhance catalytic activity, so a large number of supports have been researched, for example,  $\text{SiO}_2$ ,  $\text{CeO}_2$ ,  $\text{Al}_2\text{O}_3$  and so on [16,17].

Graphitic carbon nitride (g-C<sub>3</sub>N<sub>4</sub>) is a promising catalytic materials [18-20], and the rich nitrogen content supplies abundant anchoring sites for metallic nanoparticles when g-C<sub>3</sub>N<sub>4</sub> is used as heterogeneous catalyst support [21]. In addition, g-C<sub>3</sub>N<sub>4</sub> provides a large amount of active sites for catalytic reactions because it is a Lewis base catalyst derived from incompletely condensed amino functions together with tertiary and aromatic amines. And when metal nanoparticles and g-C<sub>3</sub>N<sub>4</sub> coexist, it can produce delocalized electron which are favorable for catalytic reactions. More importantly, it is deeply tolerant to temperature and toxic chemicals because of its s-triazine ring structure and high condensation degree [22]. Thus, g-C<sub>3</sub>N<sub>4</sub> is not only a carrier, but also an “active support”, enhancing the catalytic performance of catalyst. Its properties have been proved by the application of various fields [23,24].

Herein, in order to combine the advantages of Co-N-C and g-C<sub>3</sub>N<sub>4</sub> to synthesize catalysts with better catalytic performance, we successfully prepare Co-N-C/g-C<sub>3</sub>N<sub>4</sub> through the pyrolysis of different amount of cobalt (II) 5,10,15,20-tetraphenylporphyrin immobilized on graphitic carbon nitride in N<sub>2</sub> atmosphere. Characterization methods such as UV-vis, FT-IR, TG-DTA, XRD, SEM, TEM, HRTEM, BET and XPS are employed to investigate their physicochemical properties. Furthermore, the performance of the catalysts was investigated using selective oxidation of ethylbenzene with molecular oxygen as oxidant.

## **2. Experimental**

### *2.1. Materials*

Melamine, pyrrole, benzaldehyde, propionic acid, ethanol, *N,N*-dimethyl formamide (DMF), cobalt chloride hexahydrate (CoCl<sub>2</sub>·6H<sub>2</sub>O), dichloromethane (CH<sub>2</sub>Cl<sub>2</sub>), ethylbenzene, bromobenzene, 1,4-dichlorobenzene were obtained commercial sources and used as received without further purification. Deionized (DI) water was homemade.

### *2.2. Catalysts preparation*

#### *2.2.1. Synthesis of cobalt (II) 5,10,15,20-tetraphenylporphyrin (CoTPP).*

The cobalt (II) 5,10,15,20-tetraphenylporphyrin was obtained as described in a literature [25]. At first, benzaldehyde (5.56 g) was added into propionic acid (200 mL) and stirred gently at 130 °C in a dry 500 mL three necked flask, then pyrrole (2.62 g) in propionic acid (20 mL) was carefully added dropwise with a dropping funnel, and the mixture was kept at 130 °C for 1 h under magnetic stirring. As the temperature was cooled down to room temperature, the purple precipitate (5,10,15,20-tetraphenylporphyrin) was obtained through vacuum suction filtration, followed by washing with DI water and ethanol, purifying by column chromatography, and drying in an oven at 80 °C for overnight. Subsequently, as-obtained product (1.0 g) and  $\text{CoCl}_2 \cdot 6\text{H}_2\text{O}$  (2.5 g) were dissolved into DMF (100 mL) in a dry 250 mL round-bottomed flask, and then refluxed for 1 h at 120 °C with stirring. After cooling to the room temperature, the 100 mL DI water added and then refrigerated overnight. The precipitates were filtered, washed by DI water and dried at 80 °C. The brick-red solids cobalt (II) 5,10,15,20-tetraphenylporphyrin (CoTPP) was obtained.

### 2.2.2. Synthesis of *g*- $\text{C}_3\text{N}_4$

The *g*- $\text{C}_3\text{N}_4$  could be prepared by thermal polymerization method [18]. In this typical procedure, melamine in an open crucible was heated in static air with a heating rate of 2 °C/min to 550 °C and kept for 4 h, then cooled naturally to room temperature. The as-obtained yellow solid was finely ground into powder to subsequent processes.

### 2.2.3. Synthesis of *Co-N-C* and *Co-N-C*/*g*- $\text{C}_3\text{N}_4$

Typically, CoTPP was loaded in crucible and pyrolyzed at 550 °C for 1 h under  $\text{N}_2$  atmosphere with a heating rate 10 °C/min. The as-received black powder was denoted as *Co-N-C*. 200 mg of *g*- $\text{C}_3\text{N}_4$  and different amounts (1, 2, 6, 10, 20, 40 and 100 mg) of CoTPP were dissolved in 10 mL of  $\text{CH}_2\text{Cl}_2$  solvent under sonicating, and the mixture was stirred for 10 h at 45 °C. The solvent was removed using a rotary evaporator and then dried in an oven at 80 °C. After grinding, the powder was transferred into a crucible and heated at 550 °C for 1 h under  $\text{N}_2$  atmosphere with a heating rate 10 °C/min. After that, the sample was naturally cooled down to room

temperature. At last, the as-obtained catalyst (designated as Co-N-C<sub>x</sub>/g-C<sub>3</sub>N<sub>4</sub>, where x refers to the mass ratio of CoTPP to g-C<sub>3</sub>N<sub>4</sub>, *i.e.*, x = 0.005, 0.01, 0.03, 0.05, 0.1, 0.2 and 0.5) was ground into powder for further use.

### 2.3. Catalytic activity measurements

The catalytic activity of the catalysts for the oxidation of ethylbenzene was carried out in a Teflon-lined stainless steel batch reactor (50 mL total volume) with a magnetic stirrer, which contained 30 mg of catalyst and 10 mL of ethylbenzene. And then the reactor was sealed and filled with oxygen (0.8 MPa) as oxidant. The reaction was then kept at 120 °C for 5 h under stirring. The compositions of products were analyzed using a Shimadzu GC-2014 with an internal standard method, bromobenzene and 1,4-dichlorobenzene as references. Finally, the catalyst was recovered *via* centrifugation and washed with ethanol, then dried in an oven at 80 °C for overnight in order to further use to test the reusability and durability. After recycling 6 times, the catalyst (denoted as catalyst R6, *i.e.*, Co-N-C<sub>0.2</sub>/g-C<sub>3</sub>N<sub>4</sub> R6), was collected for further experiments.

### 2.4. Characterization

Ultraviolet–visible spectroscopy (UV-vis) diffuse reflectance spectra of solid samples were collected on the Shimadzu 2450 spectrophotometer. FT-IR (Fourier Transform Infrared) was conducted on a Vertex 70 (Bruker) spectrometer. TG-DTA was measured by a Shimadzu TG/DTA 60 thermal analyzer. X-Ray diffraction patterns (XRD) were carried out on Japan XRD-6100 diffractometer using Ni-filtered Cu K $\alpha$  radiation (50 kV and 10 mA). The morphology of the samples was investigated by field emission scanning electron microscopy (SEM) (JSM-6700F). Transmission electron microscope (TEM) was performed on JEM-3010 high resolution transmission electron microscope operating at 200 KV. Surface area was measured by nitrogen adsorption/desorption at 77 K on a NOVA 1000e apparatus from Quantachrome Instruments. The samples were degassed at 300 °C for 3 h prior to the adsorption experiments. The Brunauer-Emmett-Teller (BET) was used to

determine the specific surface areas and pore volume. The Barrett-Joyner-Halenda (BJH) method was useful for determining mesopore size distribution of the samples. X-ray photoelectron spectra (XPS) was conducted on PHI 5000 CESCAs system (Perkin Elmer) using an Al K $\alpha$  X-ray source to detect the elemental composition of catalysts. The binding energies were calibrated with the C1s peak at 284.6 eV as standard.

### **3.Results and Discussion**

We have reported that nitrogen-doped carbon cobalt catalysts with SiO<sub>2</sub>, CeO<sub>2</sub>, Al<sub>2</sub>O<sub>3</sub> and Fe<sub>2</sub>O<sub>3</sub> as support [14,17]. In this work, we successfully prepare Co-N-C/g-C<sub>3</sub>N<sub>4</sub> catalyst, and the fabrication process using cobalt porphyrin as precursor and g-C<sub>3</sub>N<sub>4</sub> as support is illustrate in Scheme 1. It can be directly observed the color variation from a series of Co-N-C/g-C<sub>3</sub>N<sub>4</sub> catalysts (Fig. S1). And FT-IR spectra and UV-vis spectra were carried out for testifying our synthetic strategy (Fig. S2 and Fig. S3).

#### *3.1. Catalyst characterization*

##### *3.1.1 TG-DTA*

In order to investigate the thermal stability of CoTPP and g-C<sub>3</sub>N<sub>4</sub>, TG-DTA has been conducted (Fig. 1). As depicted in Fig. 1a, the TG-DTA curves describe the heat-treatment procedure of CoTPP, and different stages can be observed. Initially, the slight weight loss is due to the dehydration below 340 °C. When the temperature is raised to 470 °C, carbon oxides are released because of polymerization of metalloporphyrin. Porphyrin polymers are decomposed at 470-545 °C, Co-N-C and Co-N<sub>x</sub> are formed during this period. When the temperature higher than 545 °C, it will produce a great deal of Co-N-C, Co-N<sub>x</sub> and graphite carbon [15]. Finally, Co-N<sub>x</sub> and CoO<sub>x</sub> are responsible for the weight loss at temperature higher than 735 °C [16]. As for Fig.1b, it is obvious that g-C<sub>3</sub>N<sub>4</sub> has superior stability at 550 °C, indicating that it is suitable to serve as support.

##### *3.1.2. XRD*

The chemical structure of the  $g\text{-C}_3\text{N}_4$ , Co-N-C and Co-N- $\text{C}_x/g\text{-C}_3\text{N}_4$  ( $x = 0.005$ , 0.2 and 0.5) were corroborated by X-ray diffraction pattern (XRD). As shown in Fig. 2, the diffraction peaks of Co-N-C at  $44.2^\circ$ ,  $51.5^\circ$  and  $75.8^\circ$  are ascribed to the characteristic (111), (200) and (220) reflections of Co (PDF 15-0806), respectively [26]. We can also observe the weak peaks at  $36.5^\circ$ ,  $42.4^\circ$  and  $61.5^\circ$ , which can be indexed to the crystalline facets (111), (200) and (220) of CoO (PDF 43-1004), respectively. The broad peak at  $26.4^\circ$  represents the presence of low-crystallinity carbon. Besides, two obviously characteristic peaks are observed in the spectra of  $g\text{-C}_3\text{N}_4$ . The peak at  $13.1^\circ$  can be attributed to the (100) peak and the in-plane structural packing motif of triazine units, corresponding to an interlayer distance of 0.675 nm. Another strong peak at  $27.5^\circ$  is ascribed to the interlayer stacking of aromatic segments with a  $d = 0.324$  nm interlayer distance and the (002) peak of the conjugated aromatic stacking [18]. Interestingly, the intensity of (002) peaks from Co-N- $\text{C}_{0.5}/g\text{-C}_3\text{N}_4$  to  $g\text{-C}_3\text{N}_4$  becomes significantly weaker, it seems to be mainly due to the presence of the Co-containing species that seem to impede the  $g\text{-C}_3\text{N}_4$  layer stacking. The relatively lower peak intensity of (002) also means a lower graphitization degree of catalysts [27]. Nevertheless, no characteristic diffraction peaks for Co can be observed in the XRD patterns of Co-N- $\text{C}_x/g\text{-C}_3\text{N}_4$  due to its low content in the composites and a good dispersion on the  $g\text{-C}_3\text{N}_4$  support.

### 3.1.3. SEM&TEM

The morphology and components of these catalysts were investigated by scanning electronic microscopy (SEM) and transmission electron microscopy (TEM) in Fig. 3 and high resolution transmission electron microscopy (HRTEM) in Fig. S5. As can be seen, the  $g\text{-C}_3\text{N}_4$  is composed of irregular large size solid agglomerates (Fig. 3a). As shown in Fig. 3b, there are some differences for the morphology between Co-N- $\text{C}_{0.2}/g\text{-C}_3\text{N}_4$  and  $g\text{-C}_3\text{N}_4$ , it is due to Co-N-C immobilizes on the  $g\text{-C}_3\text{N}_4$  support. In TEM image of Co-N-C (Fig. 3c), cobalt nanoparticles with a mean size of 7.24 nm (Fig. S5a) are observed and uniformly dispersed in the carbon matrix. The lattice fringe spaces are measured by HRTEM to be 0.240 nm, which is in good agreement

with the (111) facet of crystalline CoO (Fig. S5b). Compared with pure Co-N-C, cobalt nanoparticles can not be observed in the TEM images of Co-N-C/g-C<sub>3</sub>N<sub>4</sub> (Fig. 3d-f), which may be due to a good dispersion caused by the immobilization of CoTPP onto g-C<sub>3</sub>N<sub>4</sub>. In addition, the Co<sub>2</sub>O<sub>3</sub> planes of Co-N-C<sub>0.5</sub>/g-C<sub>3</sub>N<sub>4</sub> with lattice fringe spaces 0.324 nm are observed (Fig. S5d). Furthermore, the morphology of recycled Co-N-C<sub>0.2</sub>/g-C<sub>3</sub>N<sub>4</sub> after using 6 times was also investigated. As shown in Fig. 3g, many hollow circles can be observed, and it also shows that cobalt oxides have an average size of 7.08 nm with sizes ranging from 5 to 9 nm, and its lattice fringe spaces of 0.324 and 0.240 nm are attributed to the Co<sub>2</sub>O<sub>3</sub> and CoO crystal, respectively (Fig. S5f).

#### 3.1.4. BET

The specific surface area of Co-N-C<sub>0.2</sub>/g-C<sub>3</sub>N<sub>4</sub> and corresponding pore size distribution was investigated by nitrogen adsorption/desorption isotherm. As shown in Fig. 4, the adsorption isotherm resembles type IV with a hysteresis loop, indicating that the presence of mesoporous structure. From Table 1, the average pore size of Co-N-C<sub>0.2</sub>/g-C<sub>3</sub>N<sub>4</sub> is 3.9 nm, which almost equally with the pore size of g-C<sub>3</sub>N<sub>4</sub> (4.0 nm), and the specific surface area is calculated to be 28.56 m<sup>2</sup> g<sup>-1</sup>. The specific surface areas and total pore volume of the Co-N-C<sub>x</sub>/g-C<sub>3</sub>N<sub>4</sub> (x = 0.005, 0.2 and 0.5) increase gradually with the increasing mass ratio of the cobalt porphyrin to g-C<sub>3</sub>N<sub>4</sub>. Besides, the average pore sizes of all catalysts are unchanged compared to that of pure g-C<sub>3</sub>N<sub>4</sub> and larger than that of Co-N-C. Generally, high surface area catalytic materials are expected to give better catalytic performance due to accommodate more active sites [28]. However, the activity of catalysts is not exactly in line with this law, indicating that the specific surface areas and total pore volume are not the key factors to influence the performance of catalysts. In addition, the specific surface area and total pore volume of Co-N-C<sub>0.2</sub>/g-C<sub>3</sub>N<sub>4</sub> R6 are significantly larger than Co-N-C<sub>0.2</sub>/g-C<sub>3</sub>N<sub>4</sub>, which maybe account for the generated hollow circles in TEM (Fig. 3g).

#### 3.1.5. XPS

The X-ray photoelectron spectroscopy (XPS) measurements were carried out to further determine the surface compositions and chemical states of the catalysts. C, N, O and Co elements without other impurities are displayed in the full survey spectra (Fig. 5a), indicating that carbon, nitrogen and cobalt are successfully incorporated into the catalyst of Co-N-C<sub>0.2</sub>/g-C<sub>3</sub>N<sub>4</sub>. The C1s spectrum Fig. 5a represents four peaks at the binding energies of 284.6, 285.6, 286.6 and 288.5 eV, which is assigned to C=C, C=N, C-N and O-C=O, respectively, suggesting that the existence of carbon atoms connected to N and O atoms [29]. Moreover, as shown in Fig. 5b, the high resolution N1s peaks can be fitted into four peaks at 398.6, 399.9, 401.3 and 404.4 eV, respectively. The peak at 398.6 eV can be ascribed to pyridinic N considered as the possible active sites in the oxidation of C-H bond reaction. The peak with binding energy of 399.9 eV is the characteristic peak of pyrrolic N, which is contributing two electrons to the carbon matrix and bonding to a hydrogen atom [13,17]. Other peaks at 401.3 and 404.4 eV are attributed to quaternary N and oxidized N, respectively [30]. In addition, three peaks of O1s at 529.8, 531.3 and 532.4 eV correspond to cobalt (II) oxides, carboxyls and hydroxyls, respectively (Fig. 5c) [31]. As manifested in Fig. 5d, two core-level signals located at 779.5 and 795.1 eV are attributed to Co2p<sub>3/2</sub> and Co2p<sub>1/2</sub>, respectively. After deconvolution, three satellite peaks are observed, which are characteristic feature of cobalt oxides (e.g. CoO, Co<sub>2</sub>O<sub>3</sub> and Co<sub>3</sub>O<sub>4</sub>), Co(III) at the binding energies of 779.1 eV and 794.4 eV, and Co(II) at the binding energies of 780.8 eV and 796.5 eV [32]. The peak at 779.5 eV and 795.1 eV are assigned to Co<sub>3</sub>O<sub>4</sub> phase [12,25,33]. However, we can not find the Co<sub>3</sub>O<sub>4</sub> from XRD and HRTEM, indicating that Co<sub>3</sub>O<sub>4</sub> a low content and the presence of a good dispersion. The dominant existence of Co (III) oxides in the XPS analysis reveals that the Co nanoparticles on the surface of this catalyst are severely oxidized.

Table 2 lists out the content of various elements, evidently, the element of C is the dominant phase. Furthermore, the content of C in the Co-N-C<sub>x</sub>/g-C<sub>3</sub>N<sub>4</sub> (x = 0.005, 0.2 and 0.5) increases with the increasingly content of cobalt porphyrin, while that of N content decreased. All nitrogen species from cobalt porphyrin are pyrrolic N, but

high temperature carbonization leads to the presence of pyridinic N, quaternary N and oxidized N. The content of pyridinic N is higher than pyrrolic N, indicating that pyridinic N can effectively enhance the activity of catalysts to some degree [34]. It is noteworthy that there is no monotonic relationship between the total content of N and catalytic activity, although properly doped nitrogen can enhance catalytic performance [35]. Both pyridinic N and pyrrolic N can coordinate with Co [36,37], which can produce Co-N<sub>x</sub> active site at high temperature. Moreover, pyridinic N and pyrrolic N are the dominant phases in these catalysts, thus, more Co-N<sub>x</sub> active sites are produced and more favorable for catalytic performance. From Table S1, there are little differences in the amount of pyridinic N, pyrrolic N and quaternary N before and after reaction, suggesting that there is no significant change in the amount of Co-N<sub>x</sub> active sites, it further evidences of the superior catalytic performance of Co-N-C<sub>0.2</sub>/g-C<sub>3</sub>N<sub>4</sub>.

### 3.2. Catalytic performance

In order to investigate the catalytic performance of catalysts, selective oxidation of ethylbenzene to acetophenone using O<sub>2</sub> as oxidant at 120 °C and 0.8 MPa pressure was conducted, as shown in Table 3. Compared with Co-N-C<sub>x</sub>/g-C<sub>3</sub>N<sub>4</sub> (x = 0.005, 0.01, 0.03, 0.05, 0.1, 0.2 and 0.5), the control groups of Co-N-C and g-C<sub>3</sub>N<sub>4</sub> show poor conversion of ethylbenzene. Thus, it can be speculated that the metal carbon nitrogen (Co-N-C), as well as the synergistic effect between Co-N-C and g-C<sub>3</sub>N<sub>4</sub>, may play a vital role in the reaction. And interestingly, the catalytic activity of the corresponding catalysts for ethylbenzene conversion presents a normal distribution curve when the content of cobalt porphyrin over g-C<sub>3</sub>N<sub>4</sub> support increased successively. As a result, Co-N-C<sub>0.005</sub>/g-C<sub>3</sub>N<sub>4</sub>, Co-N-C<sub>0.2</sub>/g-C<sub>3</sub>N<sub>4</sub> and Co-N-C<sub>0.5</sub>/g-C<sub>3</sub>N<sub>4</sub> with the ethylbenzene conversion of 16.2%, 28.0% and 20.1%, respectively, which is due to a different degree of agglomeration from cobalt nanoparticles and hindering electron transport between the carbon matrix and the cobalt nanoparticles [38].

Moreover, these catalysts can be easily separated and recovered from the

reaction solvent only by simple centrifugation. The reusability of Co-N-C<sub>0.2</sub>/g-C<sub>3</sub>N<sub>4</sub> was investigated (Fig. 6), and it exhibits better recyclability after recycling 6 times. As a result, the selectivity of acetophenone is nearly unchanged after recycling the first time but the conversion of ethylbenzene declines slightly, it is due to the content of Co (III) decreases whereas Co (II) increases (Table S1) [17]. It reveals that the catalyst with g-C<sub>3</sub>N<sub>4</sub> support is beneficial for reusability, because g-C<sub>3</sub>N<sub>4</sub> can afford sufficient nitrogen which usually has a lone pair of electrons with strongly electronegative. Nitrogen on the catalysts surface might act as Lewis base sites and is expected to be more effective in retaining metal nanoparticles [39]. Compared with Co-N-C<sub>0.2</sub>/g-C<sub>3</sub>N<sub>4</sub>, Co-N-C-600/SiO<sub>2</sub>, Co-N-C/Al<sub>2</sub>O<sub>3</sub> and Co-N-C/Fe<sub>2</sub>O<sub>3</sub> display poor conversion of ethylbenzene. Although Co-N-C/CeO<sub>2</sub> has slightly higher conversion, it exhibits poor stability in the reported literature [17], thus, we can conclude the g-C<sub>3</sub>N<sub>4</sub> support is more favorable for the activity and stability of Co-N-C catalyst. This result indicating that a series of Co-N-C/g-C<sub>3</sub>N<sub>4</sub> are reasonable and environmental friendly catalysts for selective oxidation of ethylbenzene to acetophenone under this mild reaction conditions.

#### 4. Conclusions

To sum up, a series of Co-N-C/g-C<sub>3</sub>N<sub>4</sub> were prepared *via* a simple heating method under N<sub>2</sub> atmosphere and their catalytic performance of selective aerobic oxidation of ethylbenzene to acetophenone with solvent-free was investigated. The catalysts display superior performance, indicated that the Co-N-C modification with g-C<sub>3</sub>N<sub>4</sub> support can significantly enhance the catalytic performance. Moreover, when the mass ratio of cobalt porphyrin to g-C<sub>3</sub>N<sub>4</sub> is 20%, the conversion of ethylbenzene reached 2.3 and 1.9 times higher than pure g-C<sub>3</sub>N<sub>4</sub> and Co-N-C, respectively. According to various characterizations, the reason for enhancing the catalytic activity is ascribed to the Co-N<sub>x</sub> active site and the synergistic effect between Co-N-C and g-C<sub>3</sub>N<sub>4</sub>. In addition, the catalyst of Co-N-C<sub>0.2</sub>/g-C<sub>3</sub>N<sub>4</sub> possesses better durability after recycling 6 times under the same reaction conditions. Therefore, nitrogen-doped carbon cobalt grafted on graphitic carbon nitride catalysts would have more hopeful

prospects in catalytic applications.

### **Acknowledgments**

The authors gratefully acknowledge the financial support from National Natural Science Foundation of China (No. 21103045, 1210040, 1103312), the Fundamental Research Funds for the Central Universities, the State Key Laboratory of Heavy Oil in China (No. SKCHOP201504) and the Key Laboratory of Mineralogy and Metallogeny in Chinese Academy of Sciences (No. KLMM20150103).

## References

- [1] R. Liu, S. M. Mahurin, C. Li, R. R. Unocic, J. C. Idrobo, H. J. Gao, S. J. Pennycook, S. Dai, *Angew. Chem., Int. Ed.* 50 (2011) 6799.
- [2] Z. Wei, Y. Gong, T. Xiong, P. Zhang, H. Li, Y. Wang, *Catal. Sci. Technol.* 5 (2015) 397.
- [3] D. Jariwala, V. K. Sangwan, L. J. Lauhon, T. J. Marks, M. C. Hersam, *Chem. Soc. Rev.* 42 (2013) 2824.
- [4] Y. Su, J. Lang, L. Li, K. Guan, C. Du, L. Peng, D. Han, X. Wang, *J. Am. Chem. Soc.* 135 (2013) 11433.
- [5] D. Gärtner, A. Welther, B. R. Rad, R. Wolf, A. J. Wangelin, *Angew. Chem. Int. Ed.* 53 (2014) 3722.
- [6] T. Punniyamurthy, S. Velusamyand, J. Iqbal, *Chem. Rev.* 105 (2005) 2329.
- [7] J. M. Thomas, R. Raja, G. Sankar, R. G. Bell, *Nature* 398 (1999) 227.
- [8] M. Arshadi, M. Ghiaci, A. A. Ensafi, H. K. Maleh, S. L. Suib, *J. Mol. Catal. A: Chem.* 338 (2011) 71.
- [9] V. R. Choudhary, J. R. Indurkar, V. S. Narkhede, R. Jha, *J. Catal.* 227 (2004) 257.
- [10] A. K. Suresh, M. M. Sharma, T. Sridhar, *Ind. Eng. Chem. Res.* 39 (2000) 3958.
- [11] J. Sanetuntikul, S. Shanmugam, *Nanoscale* 7 (2015) 7644.
- [12] Z. Wei, J. Wang, S. Mao, D. Su, H. Jin, Y. Wang, F. Xu, H. Li, Y. Wang, *ACS Catal.* 5 (2015) 4783.
- [13] H. W. Liang, W. Wei, Z. S. Wu, X. L. F. K. Müllen, *J. Am. Chem. Soc.* 135 (2013) 16002.
- [14] Z. Liu, L. Ji, X. Dong, Z. Li, L. Fu, Q. Wang, *RSC Adv.* 5 (2015) 6259.
- [15] L. Fu, Y. Chen, Z. Liu, *J. Mol. Catal. A: Chem.* 408 (2015) 91.

- [16] Z. Liu, L. Ji, J. Liu, L. Fu, S. Zhao, *J. Mol. Catal. A: Chem.* 395 (2014) 315.
- [17] Y. Chen, S. Zhao, Z. Liu, *Phys. Chem. Chem. Phys.* 17 (2015) 14012.
- [18] L. Liu, Y. Qi, J. Lu, S. Lin, W. An, Y. Liang, W. Cui, *Appl. Catal. B: Environ.* 183 (2016) 133.
- [19] S. Cao, J. Yu, *J. Phys. Chem. Lett.* 5 (2014) 2101.
- [20] S. Yang, Y. Gong, J. Zhang, L. Zhan, L. Ma, Z. Fang, R. Vajtai, X. Wang, P. M. Ajayan, *Adv. Mater.* 25 (2013) 2452.
- [21] Y. Wang, J. Yao, H. R. Li, D. S. Su, M. Antonietti, *J. Am. Chem. Soc.* 133 (2011) 2362.
- [22] Y. Wang, X. Wang, M. Antonietti, *Angew. Chem. Int. Ed.* 51 (2012) 68.
- [23] F. Goettmann, A. Fischer, M. Antonietti, A. Thomas, *Angew. Chem. Int. Ed.* 45 (2006) 4467.
- [24] Y. Tian, B. Chang, J. Lu, J. Fu, F. Xi, X. Dong, *ACS Appl. Mater. Interfaces* 5 (2013) 7079.
- [25] Y. Chen, L. Fu, Z. Liu, *Chem. Commun.* 51 (2015) 16637.
- [26] Y. Wu, J. Zang, L. Dong, Y. Zhang, Y. Wang, *J. Power Sources* 305 (2016) 64.
- [27] B. Qiu, C. Pan, W. Qian, Y. Peng, L. Qiu, F. Yan, *J. Mater. Chem. A* 1 (2013) 6373.
- [28] Y. Xing, *J. Phys. Chem. B* 108 (2004) 19255.
- [29] Y. Su, Y. Zhu, H. Jiang, J. Shen, X. Yang, W. Zou, J. Chen, C. Li, *Nanoscale* 6 (2014) 15080.
- [30] H. Xiao, Z. Shao, G. Zhang, Y. Gao, W. Lu, B. Yi, *Carbon* 57 (2013) 443.
- [31] V. Datsyuk, M. Kalyva, K. Papagelis, J. Parthenios, D. Tasis, A. Siokou, I. Kallitsis, C. Galiotis, *Carbon* 46 (2008) 833.

- [32] J. F. Macro, J. R. Gancedo, M. Gtacia, J. L. Gautier, E. I. Rios, H. M. Palmer, C. Greaves, F. J. Berry, *J. Mater. Chem.*, 11 (2001) 3087.
- [33] M. C. Biesingera, B. P. Payne, A. P. Grosvenor, L. W. M. Laua, A. R. Gersonb, R. S. C. Smartb, *Appl. Surf. Sci.* 257 (2011) 2717.
- [34] K. Niu, B. Yang, J. Cui, J. Jin, X. Fu, Q. Zhao, J. Zhang, *J. Power Sources* 243 (2013) 65.
- [35] J. Luo, F. Peng, H. Wang, H. Yu. *Catal. Commun.* 39 (2013) 44.
- [36] X. Li, H. Wang, J. T. Robinson, H. Sanchez, G. Diankov, H. Dai, *J. Am. Chem. Soc.* 131 (2009) 15939.
- [37] Z. Wu, L. Chen, J. Liu, K. Parvez, H. Liang, J. Shu, H. Sachdev, R. Graf, X. Feng, K. Müllen, *Adv. Mater.* 26 (2014) 1450.
- [38] Y. Chen, L. Fu, Z. Liu, Y. Wang, *ChemCatChem* DOI: 10.1002/cctc.201600114.
- [39] X. Xu, Y. Li, Y. Gong, P. Zhang, H. Li, Y. Wang, *J. Am. Chem. Soc.* 134 (2012) 16987.

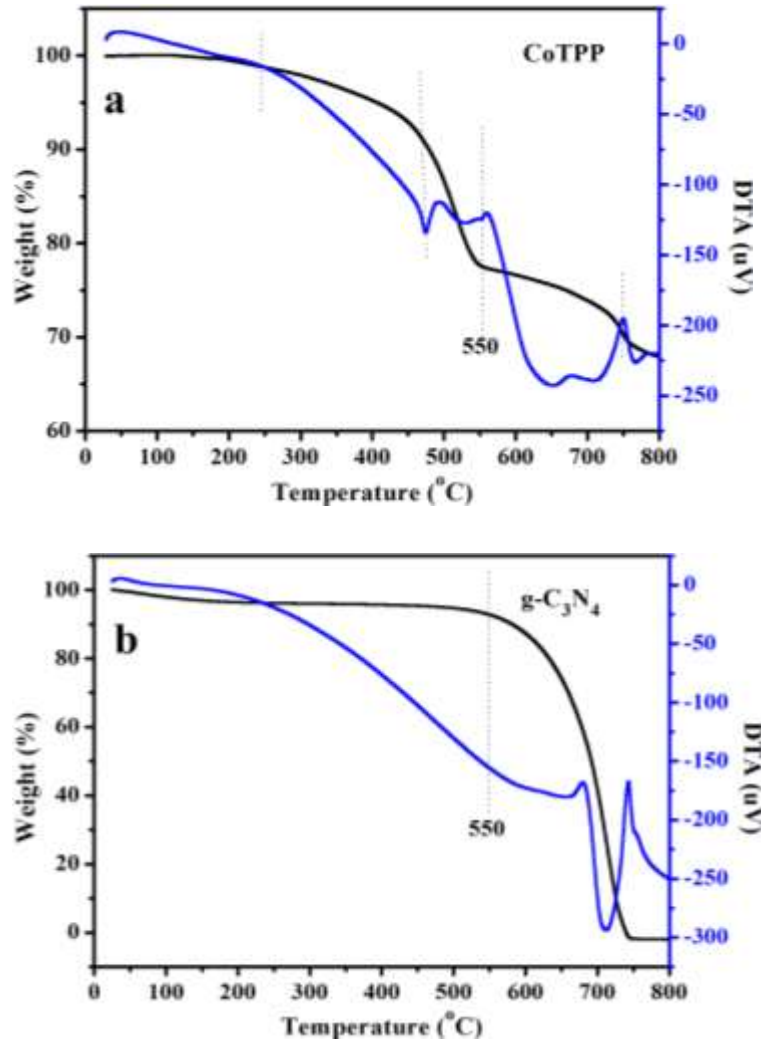


**Fig. 1.** TG-DTA curves of (a) CoTPP and (b) g-C<sub>3</sub>N<sub>4</sub>.

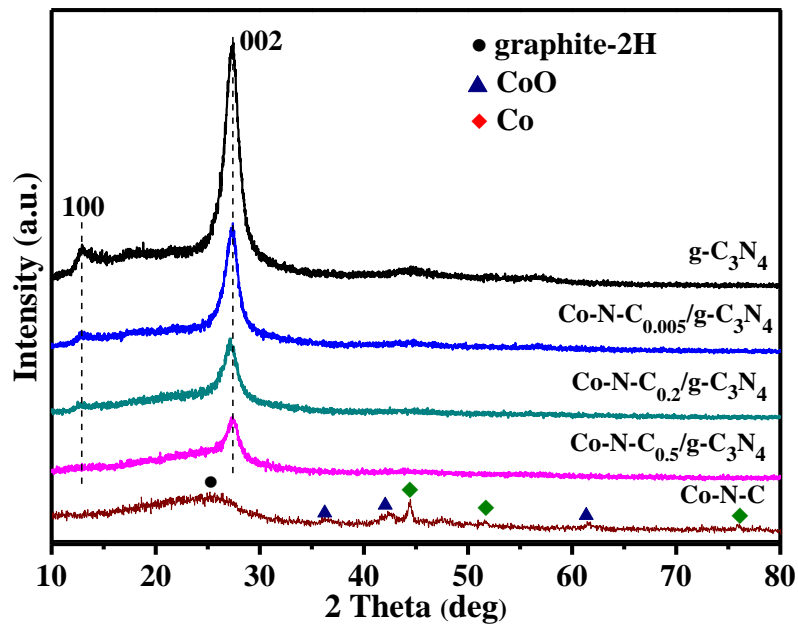


**Fig.2.** XRD patterns of g-C<sub>3</sub>N<sub>4</sub>, Co-N-C and Co-N-C<sub>x</sub>/g-C<sub>3</sub>N<sub>4</sub> (x = 0.005, 0.2 and 0.5).

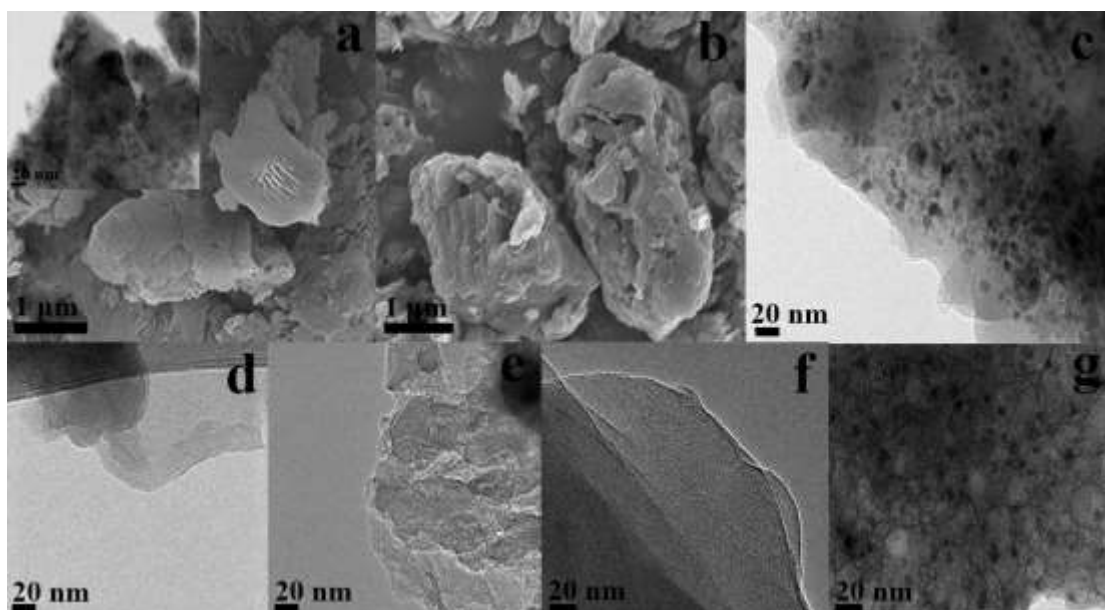


**Fig. 3.** SEM images of (a) g-C<sub>3</sub>N<sub>4</sub>, (b) Co-N-C<sub>0.2</sub>/g-C<sub>3</sub>N<sub>4</sub>; TEM images of (a) g-C<sub>3</sub>N<sub>4</sub> (inset on left top), (c) Co-N-C, (d) Co-N-C<sub>0.005</sub>/g-C<sub>3</sub>N<sub>4</sub>, (e) Co-N-C<sub>0.2</sub>/g-C<sub>3</sub>N<sub>4</sub>, (f) Co-N-C<sub>0.5</sub>/g-C<sub>3</sub>N<sub>4</sub> and (g) Co-N-C<sub>0.2</sub>/g-C<sub>3</sub>N<sub>4</sub> R6 (recycling 6 times at the same reaction conditions).

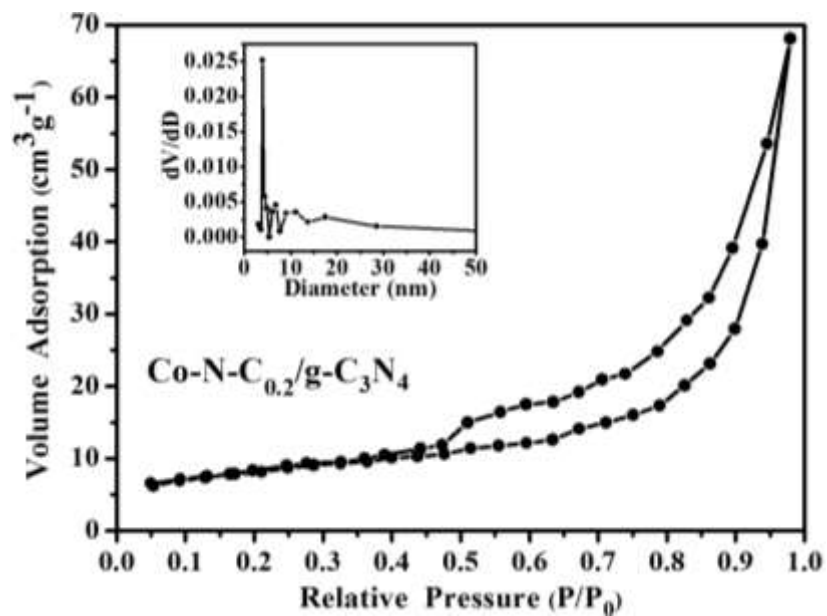


**Fig. 4.** N<sub>2</sub> adsorption/desorption isotherm plot and BJH pore size distribution (inset on left top) of Co-N-C<sub>0.2</sub>/g-C<sub>3</sub>N<sub>4</sub>.

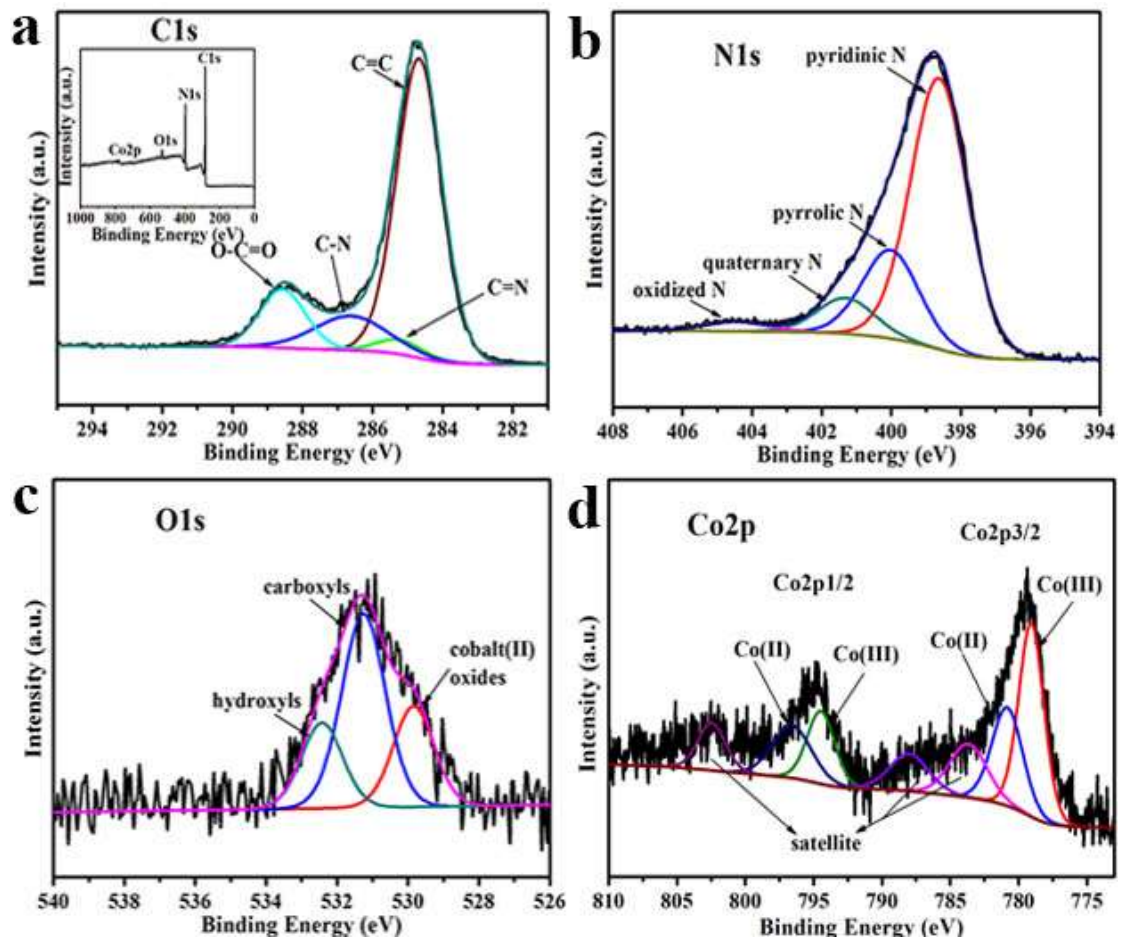


**Fig. 5.** XPS spectrum of Co-N-C<sub>0.2</sub>/g-C<sub>3</sub>N<sub>4</sub>, the high resolution of (a) C1s, inset on left top: the full survey, (b) N1s, (c) O1s, (d) Co2p, respectively.

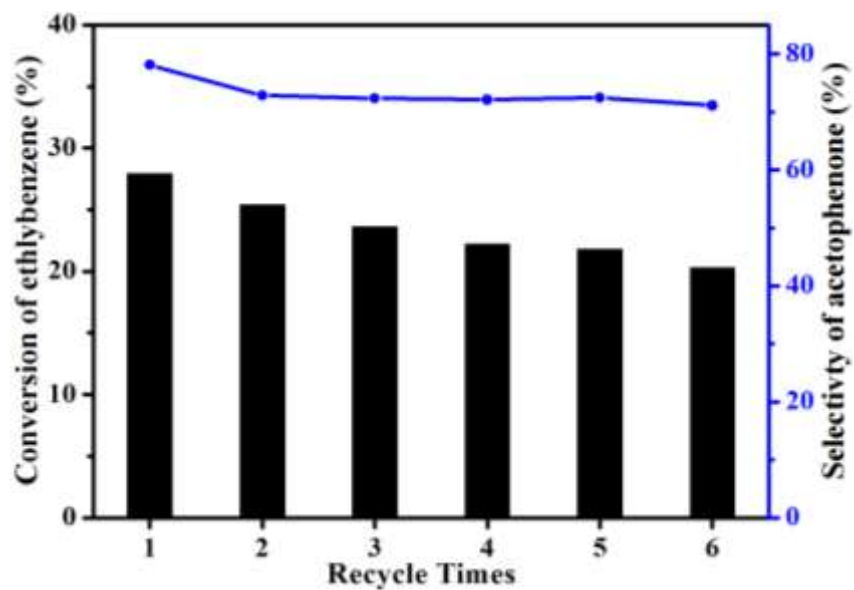
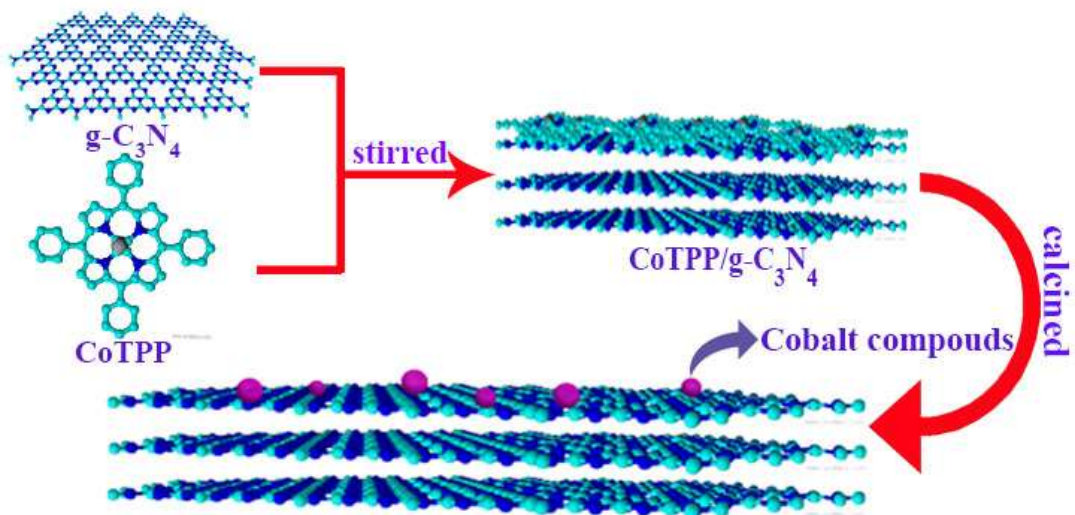


**Fig. 6.** Reusability of Co-N-C<sub>0.2</sub>/g-C<sub>3</sub>N<sub>4</sub> for ethylbenzene selective oxidation. Reaction conditions: catalyst 30 mg, ethylbenzene 10 mL, O<sub>2</sub> pressure 0.8 MPa, temperature 120 °C, reaction time 5 h.



**Scheme 1.** Schematic illustration of the preparation of Co-N-C/g-C<sub>3</sub>N<sub>4</sub>.

**Table 1:** Physical properties of g-C<sub>3</sub>N<sub>4</sub>, Co-N-C and Co-N-C<sub>x</sub>/g-C<sub>3</sub>N<sub>4</sub> (x = 0.005, 0.2 and 0.5).

Entry	Catalyst	S <sub>BET</sub> <sup>a</sup> (m <sup>2</sup> g <sup>-1</sup> )	V <sub>tot</sub> <sup>b</sup> (cm <sup>3</sup> g <sup>-1</sup> )	D <sub>p</sub> <sup>c</sup> (nm)
1	g-C <sub>3</sub> N <sub>4</sub>	10.8	0.038	4.0
2	Co-N-C <sub>0.005</sub> /g-C <sub>3</sub> N <sub>4</sub>	24.7	0.084	4.0
3	Co-N-C <sub>0.2</sub> /g-C <sub>3</sub> N <sub>4</sub>	28.6	0.105	3.9
4	Co-N-C <sub>0.5</sub> /g-C <sub>3</sub> N <sub>4</sub>	37.3	0.154	4.0
5	Co-N-C	14.5	0.016	3.3
6	R6 <sup>d</sup>	44.2	0.125	4.0

<sup>a</sup> Surface areas calculated using the BET method.

<sup>b</sup> Total pore volumes estimated from the N<sub>2</sub> adsorption isotherms at P/P<sub>0</sub> = 0.98.

<sup>c</sup> Mesopore diameters calculated from the N<sub>2</sub> desorption branches using the BJH method.

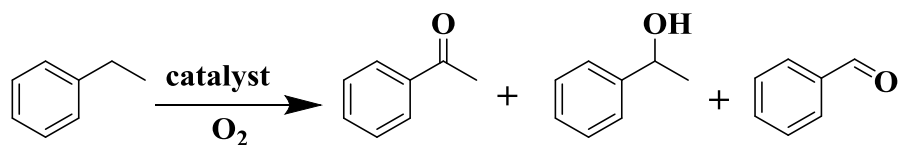
<sup>d</sup> Co-N-C<sub>0.2</sub>/g-C<sub>3</sub>N<sub>4</sub> recycling 6 times at the same reaction condition.

**Table 2:** Ratio analysis of various elements.

Entry	Catalyst	C (at%)	O (at%)	Co (at%)	N (at%)				
					total	N1 <sup>a</sup>	N2 <sup>a</sup>	N3 <sup>a</sup>	N4 <sup>a</sup>
1	g-C <sub>3</sub> N <sub>4</sub>	54.28	3.56	-	42.16	71.43	15.71	10.00	2.86
2	Co-N-C <sub>0.005</sub> /g-C <sub>3</sub> N <sub>4</sub>	56.16	2.92	0.26	40.92	70.91	14.89	11.36	2.84
3	Co-N-C <sub>0.2</sub> /g-C <sub>3</sub> N <sub>4</sub>	72.46	2.57	0.62	24.35	64.93	24.02	8.45	2.60
4	Co-N-C <sub>0.5</sub> /g-C <sub>3</sub> N <sub>4</sub>	77.91	1.88	0.72	19.49	57.47	27.59	11.49	3.45
5	Co-N-C	89.74	4.36	1.00	4.90	58.82	21.76	15.29	4.13

<sup>a</sup> N1, N2, N3, N4 represent pyridinic N, pyrrolic N, quaternary N and oxidized N, respectively.

**Table 3:** Catalytic performance of Co-N-C/g-C<sub>3</sub>N<sub>4</sub> for selective oxidation of ethylbenzene.<sup>a</sup>



Entry	Catalyst	Conversion of ethylbenzene (%)	Selectivity (%)		
			Acetophenone	Phenethyl alcohol	Benzaldehyde
1	g-C <sub>3</sub> N <sub>4</sub>	12.4	74.0	20.3	5.7
2	Co-N-C <sub>0.005</sub> /g-C <sub>3</sub> N <sub>4</sub>	16.2	74.7	20.3	5.0
3	Co-N-C <sub>0.01</sub> /g-C <sub>3</sub> N <sub>4</sub>	19.1	75.6	20.1	4.3
4	Co-N-C <sub>0.03</sub> /g-C <sub>3</sub> N <sub>4</sub>	22.3	75.0	21.7	3.3
5	Co-N-C <sub>0.05</sub> /g-C <sub>3</sub> N <sub>4</sub>	24.2	74.3	23.1	2.6
6	Co-N-C <sub>0.1</sub> /g-C <sub>3</sub> N <sub>4</sub>	27.2	77.5	20.5	2.0
7	Co-N-C <sub>0.2</sub> /g-C <sub>3</sub> N <sub>4</sub>	28.0	78.1	20.0	1.9
8	Co-N-C <sub>0.5</sub> /g-C <sub>3</sub> N <sub>4</sub>	20.1	74.2	23.0	2.8
9	Co-N-C	14.6	75.0	21.6	3.4
10	Co-N-C-600/SiO <sub>2</sub> [14]	22.9	74.9	21.7	3.4
11 <sup>b</sup>	Co-N-C/CeO <sub>2</sub> [17]	33.1	74.8	22.7	2.5
12 <sup>b</sup>	Co-N-C/Fe <sub>2</sub> O <sub>3</sub> [17]	17.8	71.5	24.9	3.6
13 <sup>b</sup>	Co-N-C/Al <sub>2</sub> O <sub>3</sub> [17]	16.2	75.0	21.1	3.9

<sup>a</sup> Reaction condition: ethylbenzene 10 mL, catalyst 30 mg, O<sub>2</sub> pressure 0.8 MPa, reaction time 5 h, temperature 120 °C.

<sup>b</sup> Catalyst 50 mg.